

Running mass, effective energy and confinement: the lattice quark propagator in Coulomb gauge

G. Burgio,¹ M. Schröck,² H. Reinhardt,¹ and M. Quandt¹

¹*Institut für Theoretische Physik, Auf der Morgenstelle 14, 72076 Tübingen, Germany*

²*Institut für Physik, FB Theoretische Physik, Universität Graz, 8010 Graz, Austria*

We calculate the lattice quark propagator in Coulomb gauge both from dynamical and quenched configurations. We show that in the continuum limit both the static and full quark propagator are multiplicatively renormalizable. From the propagator we extract the quark renormalization function $Z(|\mathbf{p}|)$ and the running mass $M(|\mathbf{p}|)$ and extrapolate the latter to the chiral limit. We find that $M(|\mathbf{p}|)$ practically coincides with the corresponding Landau gauge function for small momenta. The computation of $M(|\mathbf{p}|)$ can be however made more efficient in Coulomb gauge; this can lead to a better determination of the chiral mass and the quark anomalous dimension. Moreover from the structure of the full propagator we can read off an expression for the dispersion relation of quarks, compatible with an IR divergent effective energy. If confirmed on larger volumes this finding would allow to extend the Gribov-Zwanziger confinement mechanism to the fermionic sector of QCD.

PACS numbers: 11.15.Ha, 12.38.Gc, 12.38.Aw

Keywords: Coulomb gauge, Landau gauge, Kugo-Ojima, BRST, quark propagator, chiral condensate

I. INTRODUCTION

Thanks to considerable progress achieved in variational approaches [1–3], Hamiltonian investigations of Yang-Mills theories in Coulomb gauge [4] have seen a renewed interest in the last years. In such setup Gauß’s law on the states is explicitly resolved with the help of the gauge constraint, without any need to construct the physical Hilbert space *explicitly* [5]. The results obtained [6] agree with the Gribov-Zwanziger confinement scenario [7–9] and with the existence of a confining potential driven by topological excitations [10–12]. Lattice calculations have confirmed all qualitative and most quantitative features of the continuum analysis [13–16].

Recently, an extension of variational techniques to full QCD has been proposed in Ref. [17]. In the present paper we wish, via direct lattice calculations, to set the benchmark for future checks of such results and put forward further predictions.

A key issue in all lattice studies of pure Yang-Mills theories in Coulomb gauge has been the renormalizability of Green’s functions. Indeed it has been shown in Refs. [13–16] that for *static* correlators a non-perturbative renormalization procedure can be defined in the lattice Hamiltonian limit $a_t \rightarrow 0$. Such limit must be either taken explicitly [16] by going to anisotropic lattices [18], or it can be circumvented whenever a decoupling of the temporal and spatial dependence of the correlators is possible [13–15]. Lacking a clear picture from perturbation theory [19–21], this is the only setup we are aware of in which multiplicative renormalizability of Coulomb gauge correlators seems to be guaranteed.

We will show in this paper that, as for the gluon, the lattice Coulomb gauge static quark propagator $S(\mathbf{p}) = \int dp_4 S(p)$ is indeed renormalizable. From $S(\mathbf{p})$ the renormalization function $Z(|\mathbf{p}|)$ and the running mass $M(|\mathbf{p}|)$ can be extracted. The mass function $M(|\mathbf{p}|)$, in particular, encodes the relevant information on chiral mass

and the anomalous dimension; we will find that it basically coincides, for small momenta, with its Landau gauge counterpart. Furthermore, we also demonstrate that the *full* Coulomb propagator $S(p)$ has a trivial energy dependence. Besides making it renormalizable, this allows for a definition of a quark effective energy compatible with the confining properties of the theory.

The paper is organized as follows: Sec. II describes the general lattice setup used in our investigation; Sec. III defines the observables we will study and the requirements for their renormalizability; in Sec. IV we will give our results and discuss their consequences, while Sec. V contains our conclusions and an outlook for future work.

II. LATTICE SETUP

A. Gauge field configurations

Our calculations have been performed on nine sets of gauge field configurations generated by the MILC collaboration [22, 23], made available via the Gauge Connection [24] and analyzed using mostly the C++ toolkit FermiQCD [25]. The configurations were produced with the Symanzik-improved Lüscher-Weisz gauge action [26]. Seven out of nine sets include two light degenerate (u , d) and one heavier (s) quark flavor, while two are in the quenched approximation; all dynamical calculations used the Asqtad improved action [27]. The parameters of all sets are summarized in Table I; for the reported lattice scales and quark masses we refer to Refs. [22, 23]. The lower part of the table also contains three sets, (j) - (k) , of quenched configurations on smaller lattices used for cross checks; they were produced with the Wilson action at $\beta = 5.7, 6.0$ and 6.5 . For set (i) , due to the I/O handling of FermiQCD, our main bottleneck, we could only analyze five configurations in reasonable time; although averaging over time slices did considerably increase the

statistics, auto correlations still remained high. This is reflected in the relatively large error bars on final quantities for this lattice; we will further comment on this in Sec. IV C.

Throughout the paper a will denote the lattice spacing, x and p refer to the lattice 4-coordinate and momentum, respectively, while \mathbf{x} , \mathbf{p} denote the spatial and x_4 , p_4 the temporal position and momentum component. Repeated Greek indices indicate summation over all four Euclidean components while repeated Latin indices refer to spatial components only.

$L^3 \times T$	a [fm]	am	m [MeV]	# config.
(a) $20^3 \times 64$	0.121	0.010, 0.050	15.7, 78.9	202
(b) $20^3 \times 64$	0.121	0.020, 0.050	31.5, 78.9	50
(c) $20^3 \times 64$	0.120	0.030, 0.050	47.3, 78.9	25
(d) $20^3 \times 64$	0.119	0.040, 0.050	63.1, 78.9	25
(e) $20^3 \times 64$	0.121	–	–	66
(f) $28^3 \times 96$	0.086	0.0062, 0.031	14.0, 67.8	50
(g) $28^3 \times 96$	0.086	0.0124, 0.031	27.1, 67.8	50
(h) $28^3 \times 96$	0.086	–	–	77
(i) $64^3 \times 144$	0.060	0.0036, 0.0108	11.8, 35.3	5
(j) $16^3 \times 32$	0.170	–	–	94
(k) $16^3 \times 32$	0.093	–	–	108
(l) $16^3 \times 32$	0.045	–	–	131

TABLE I. The gauge field configurations used in this study. Sets (a)–(d) and (f)–(g) include two degenerate (u , d) quarks and one heavier (s) flavour [22, 23].

B. Gauge fixing

The continuum Coulomb gauge condition,

$$\nabla \cdot \mathbf{A} = 0 \quad (1)$$

can be realized on the lattice by maximizing the gauge functional

$$F_g[U] = \Re \sum_{i,x} \text{tr} [U_i^g(x) + U_i^g(x - \hat{i})^\dagger] \quad (2)$$

with respect to gauge transformations $g(x) \in \text{SU}(3)$, where

$$U_\mu^g(x) \equiv g(x) U_\mu(x) g(x + \hat{\mu})^\dagger. \quad (3)$$

The gauge links maximizing Eq. (2) will satisfy the discretized Coulomb gauge condition

$$\Delta^g(x) \equiv \sum_i \left(A_i^g(x) - A_i^g(x - \hat{i}) \right) = 0, \quad (4)$$

where we define the gauge fields as:

$$A_i(x) \equiv \left[\frac{U_i(x) - U_i(x)^\dagger}{2ia g_0} \right]_{\text{traceless}}. \quad (5)$$

This corresponds to Hermitian generators $T^a = \lambda^a/2$ for the Lie algebra of $\text{SU}(3)$, where λ^a are the Gell-Mann matrices.

To maximize $F_g[U]$ we employ the standard over-relaxation algorithm [28], which in the case at hand can be applied to each time-slice independently. The inversion of the Dirac operator still needs however to be performed on the whole lattice and is computationally quite expensive. This forces us to analyze less configurations than those used, say, to calculate the Coulomb operator [16], making statistics lower and raising the ratio of statistical noise to Gribov noise; we have therefore not seen, at least for this first study, any need to adopt the improved techniques first developed for Landau gauge in Refs. [29, 30] and adapted to Coulomb gauge in Refs. [13–16]. Due to the presence of fermions the part of such techniques based on center transformations and thus topologically non-trivial \mathbb{Z}_N sectors [29, 30] could have not been applied anyway.

A measure of the quality of the gauge fixing for each fixed time-slice is the average L_2 -norm of the gauge fixing violation $\Delta^g \neq 0$ [31]

$$\theta(x_4) \equiv \frac{1}{L^3 N_c} \sum_{\mathbf{x}} \text{tr} [\Delta^g(\mathbf{x}, x_4) \Delta^g(\mathbf{x}, x_4)^\dagger], \quad (6)$$

where the sum runs over all spatial sites \mathbf{x} and L^3 is the number of lattice sites in one time-slice. We have chosen to stop the over-relaxation algorithm whenever on each time-slice $\sqrt{\theta}$, the default output of the `FermiQCD` code, reached machine single-precision, $\sqrt{\theta} \lesssim 5 \cdot 10^{-7}$. Notice that in the literature (see e.g. Ref. [32]) the value of θ itself, rather than of $\sqrt{\theta}$, is often reported for the quality of the gauge fixing; in our case this corresponds to $\theta \lesssim 2.5 \cdot 10^{-13}$. A possible improvement we are considering to implement in the future is to introduce a local rather than a global observable in triggering the stopping criterion, see e.g. Ref. [29, 30], resulting in a better gauge fixing.

As usual in Coulomb gauge maximizing Eq. (2) leaves the temporal links $U_4(x)$ unfixed, i.e. we still have a gauge freedom with respect to space independent gauge transformations $g(x_4) \in \text{SU}(3)$, which leave $F_g[U]$ unaffected. One possible choice to fix the residual gauge in the continuum is to require

$$\partial_4 \int d^3x A_4(x) = 0. \quad (7)$$

Throughout this paper we will use the lattice version of Eq. (7) proposed in Ref. [13, 14], which we here call integrated Polyakov gauge (IPG) and which we have adapted to the colour group $\text{SU}(N)$. For sufficiently fine temporal lattice spacing the IPG might be considered a good approximation, on average, to the Weyl gauge $A_4 = 0$ used for the Hamiltonian approach in the continuum. For further details see Appendix A.

III. THE QUARK PROPAGATOR

A. Quark propagator in Coulomb gauge

At tree-level the inverse continuum quark propagator in Euclidean space reads:

$$S^{(0)}(p)^{-1} = i\not{p} + i\not{p}_4 + m, \quad (8)$$

where we have used Feynman's slash notation, $\not{p} \equiv \sum_i \gamma_i p_i$ and $\not{p}_4 \equiv \gamma_4 p_4$; m denotes the bare quark mass. We have explicitly separated the spatial momenta p_i from the temporal component p_4 (the energy) to make contact with the non-manifestly Euclidean invariant interacting Coulomb gauge propagator $S^{-1}(p)$. The latter could, in principle, have a more complex Dirac structure than in covariant gauges since three-dimensional (spatial) covariance allows for more possible contractions of the momentum components with elements of the Euclidean Clifford algebra. More precisely, the spatial momentum \mathbf{p} can be contracted with both the spatial Dirac matrices γ_i and the proper vector component σ_{i4} of the Euclidean tensor $\sigma_{\mu\nu} = i/2[\gamma_\mu, \gamma_\nu]$. Thus, $S^{-1}(p)$ can be decomposed into four pieces:

$$S^{-1}(p) = i\not{p}A_s(|\mathbf{p}|, p_4) + i\not{p}_4A_t(|\mathbf{p}|, p_4) + i \sum_j p_j \sigma_{j4} A_d(|\mathbf{p}|, p_4) + B_m(|\mathbf{p}|, p_4) \quad (9)$$

with scalar functions $A_s(|\mathbf{p}|, p_4)$, $A_t(|\mathbf{p}|, p_4)$, $A_d(|\mathbf{p}|, p_4)$ and $B_m(|\mathbf{p}|, p_4)$, to which we will refer as the spatial, temporal, mixed and massive component, respectively.

For our calculations of the valence quark propagator we have used Asqtad improved [27] staggered fermions [33], concentrating on the dynamical point for the unquenched configurations. In Landau gauge this choice [32, 34–38] showed not only good agreement with the conceptually cleaner but very expensive overlap fermions [39–45] but also suffered less from short-distance cutoff effects as compared to clover (improved Wilson) [46, 47] or chirally improved (CI) fermions [48].

Only for the finest lattice (set (i)) we were forced to use standard Kogut–Susskind fermions [33] due to memory limitations. For this set we have calculated the propagator with a mass equal to the two light degenerate dynamical quarks (11.8 MeV) plus four partially quenched masses up to 142.1 MeV. On the quenched configuration (h) we have used a mass of 14.0 MeV, i.e. the same as on configuration (f), in order to study the effects of dynamical quarks.

Notice that for standard staggered fermions $S(p)$ will actually be a function of $k_\mu \equiv \sin p_\mu$, while the equivalent expression for the Asqtad improved quarks can be found in Appendix B. To keep notations simple we will however write the structure functions A_s , A_t , A_d and B_m as functions of the the discrete momenta p_μ taking values in the first Brillouin zone.

B. Dispersion relation and renormalizability

From the configurations at our disposal, once any suitable gauge has been fixed, the inversion of the Dirac operator directly provides us with the regularized propagator $S_{\text{reg}}(a; p)$, which depends on the lattice spacing a . Assuming multiplicative renormalizability, such regularized propagator should be related to the renormalized one $S_\zeta(p)$ via the quark wavefunction renormalization constant Z_2 , which will depend on a and the renormalization point ζ ,

$$S_{\text{reg}}(a; p) = Z_2(\zeta; a)S_\zeta(p). \quad (10)$$

In Coulomb gauge the static propagator can be then extracted from $S_\zeta(p)$ by integrating it over p_4 . For bosonic fields such static propagator agrees, up to a constant, with the inverse of the boson's dispersion relation $\omega_B(|\mathbf{p}|)$. This connection is essential in showing e.g. that the Gribov-Zwanziger confinement scenario for the gluon is indeed realized within pure Yang-Mills theories [13–15].

In the fermionic case things are a bit more complicated. In Landau gauge, up to well understood discretization effects, the renormalized propagator $S_\zeta(p)$ was shown [32, 34–38, 48] to have indeed the expected form

$$S_\zeta(p) = \frac{Z_\zeta(p^2)}{i\not{p} + M(p^2)}, \quad (11)$$

where the only dependence on the renormalization scale ζ is through the numerator $Z_\zeta(p^2)$, while the mass function $M(p^2)$ in the denominator does not depend on the cutoff a or the renormalization scale ζ ; it is thus a renormalization group invariant.

What is the physical meaning of such propagator and where can the dispersion relation be read from? At least for the non interacting case, where $M \equiv m$ and Z is constant, we know that the inverse propagator Eq. (11) is proportional, up to a Wick rotation, to the projectors on the positive and negative energy states [49]:

$$\Lambda_\pm(p) \propto \pm\not{p} + m; \quad (12)$$

the free particle dispersion relation can now be obtained by integrating the *square* of such Euclidean propagator in the energy p_4 ,

$$\omega_F^{-1}(|\mathbf{p}|) = 2 \int \frac{dp_4}{2\pi} \frac{1}{p_4^2 + \mathbf{p}^2 + m^2} = \frac{1}{\sqrt{\mathbf{p}^2 + m^2}}. \quad (13)$$

On the other hand, Eq. (11) in the interacting case can be considered the propagator of a single quasi-particle, where M depends on the 4-momentum p . In this interpretation a projector as in Eq. (12) can still be defined by simply substituting $m \rightarrow M(p^2)$. To extract the effective energy of the quasi-particle, however, one needs to model the functional form of M and Z in order to perform the integral as in Eq. (13), since a numerical summation over p_4 would be plagued by cut-off effects [13, 14].

In Coulomb gauge, we can study both the full energy-dependent propagator as in Eq. (9) and the *static* propagator $S(\mathbf{p}) = \int dp_4 S(p)$, taking the form (see Sec. IV C):

$$S_\zeta(\mathbf{p}) = \frac{Z_\zeta(|\mathbf{p}|)}{i\mathbf{p} + M(|\mathbf{p}|)}. \quad (14)$$

What is the meaning of these quantities? Consider the free Dirac equation:

$$i\frac{\partial}{\partial t}\psi = p_4\psi = h(\mathbf{p})\psi = \gamma_4(\mathbf{p} + m)\psi, \quad (15)$$

where the one-particle Hamiltonian $h(\mathbf{p})$ coincides, up to a gamma matrix and a Wick rotation, with the free inverse static propagator (i.e. $M \equiv m$ and Z constant). We can again define the projectors $\tilde{\Lambda}_\pm$ on the positive/negative free energy states and find upon Wick rotation:

$$\begin{aligned} \tilde{\Lambda}_+(\mathbf{p}) - \tilde{\Lambda}_-(\mathbf{p}) &\propto h(\mathbf{p}) \propto S^{-1}(\mathbf{p}) \\ \tilde{\Lambda}_+(\mathbf{p}) + \tilde{\Lambda}_-(\mathbf{p}) &= 1, \end{aligned} \quad (16)$$

while the dispersion relation is given by the eigenvalues of $h(\mathbf{p})$. If we now turn on the interactions and appeal again to the quasi-particle description we will have in general:

$$h(\mathbf{p}) = \frac{1}{\rho(|\mathbf{p}|)}\gamma_4(\mathbf{p} + M(|\mathbf{p}|)) \quad (17)$$

and the (Wick rotated) static Coulomb propagator will still define the energy projectors. Moreover, if we could show for the full Euclidean Coulomb propagator a relation of the form:

$$S_\zeta(p) = \frac{Z_\zeta(|\mathbf{p}|)}{i\mathbf{p} + i\mathbf{p}_4\alpha(|\mathbf{p}|) + M(|\mathbf{p}|)} \quad (18)$$

we could, up to a constant, directly read from the integration of S^2 in p_4 the dispersion relation i.e. the effective energy of the quasi-particle:

$$\begin{aligned} \omega_F^{-1}(|\mathbf{p}|) &= 2Z_\zeta^2(|\mathbf{p}|) \int \frac{dp_4}{2\pi} \frac{1}{\alpha^2(|\mathbf{p}|)p_4^2 + \mathbf{p}^2 + M^2(|\mathbf{p}|)} \\ &= \frac{Z_\zeta^2(|\mathbf{p}|)}{\alpha(|\mathbf{p}|)\sqrt{\mathbf{p}^2 + M^2(|\mathbf{p}|)}}. \end{aligned} \quad (19)$$

To check the above conjectures we first need to extract the four dressing functions in Eq. (9) from the lattice calculation. This can be done by extending the techniques developed for Wilson and staggered fermions in Landau gauge in Refs. [34, 37]. For sake of readability all technical details have been deferred to Appendix B, where the staggered case is explicitly discussed. The adaptation of the method to Wilson and Asqtad fermions is straightforward.

C. Data cuts and averaging

Throughout this work we average over the cubic (spatial) symmetries of the lattice and the parity symmetry of the propagator $S(p) = S(-p)$. To minimize discretization artifacts caused by the breaking of rotational invariance we perform a cylinder cut on the spatial momenta [50, 51].

IV. RESULTS

A. Dirac structure

Fig. 1 shows the structure function A_d for some of the data set in Tab. I, plus one of the quenched Wilson simulation, set (k) (Fig. 1d), used as a cross check. In all cases $A_d \equiv 0$, which extends the one loop result of Ref. [52] to the non perturbative regime. We will thus ignore the mixed component in the rest of this paper and express the lattice propagator as:

$$S^{-1}(p) = ik_a A_s(|\mathbf{p}|, p_4) + ik_4 a A_t(|\mathbf{p}|, p_4) + B_m(|\mathbf{p}|, p_4), \quad (20)$$

where we denote with k_μ the dimensionless lattice momenta (see Appendix B) while the spacing a in the first two terms renders the dressing functions A_s and A_t dimensionless.

B. Energy dependence

In Refs. [13–16] it was shown that the static propagators of pure lattice gauge theory in Coulomb gauge are subject to cutoff effects in the temporal lattice spacing a_t , which lead to violations of multiplicative renormalizability. These effects can be both direct, i.e. caused by an explicit energy dependence of the correlator at hand [13–15], and indirect, i.e. caused by $\mathcal{O}(a_t)$ corrections to the spectrum of the theory [16]. In principle we cannot exclude the latter effect for the quark propagator. However, the indirect energy dependence is usually much smaller than the direct effect, and a higher statistical precision as that in the present work, combined with simulations on anisotropic lattices [18], would be required to resolve it. As for the direct energy dependence of the quark dressing functions, a quantitative measure is given by:

$$\begin{aligned} d_m(z) &= \frac{B_m(|\mathbf{p}|, p_4)}{B_m(|\mathbf{p}|, p_4^{min})} \\ d_t(z) &= \frac{A_t(|\mathbf{p}|, p_4)}{A_t(|\mathbf{p}|, p_4^{min})} \\ d_s(z) &= \frac{A_s(|\mathbf{p}|, p_4)}{A_s(|\mathbf{p}|, p_4^{min})}, \end{aligned} \quad (21)$$

which on dimensional grounds should only be functions of $z = \frac{p_4}{|\mathbf{p}|}$. In Fig. 2 we show as an example the functions of Eq. (21) for configurations sets (a) and (i), plotted as

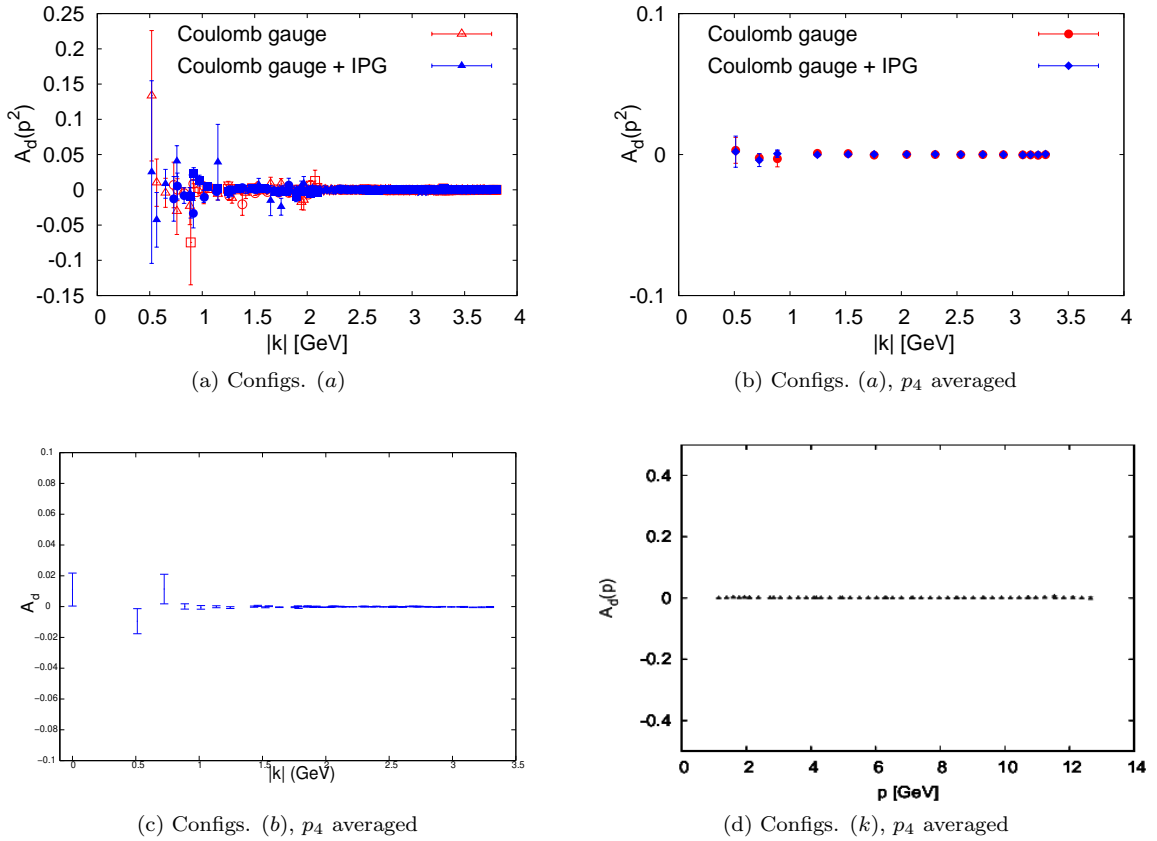


FIG. 1. Dressing function A_d . In Subfigs. 1a, 1b the effect of residual gauge fixing (IPG) is shown.

a function of $1 + z^2$ to better compare with Fig. 1 of Ref. [13].

We can conclude that, at least within our numerical precision, the functions A_s , A_t and B_m are independent of the energy p_4 . Contrary to the gluon propagator [13–15], explicit violations of renormalizability due to the temporal cutoff a_t can therefore be ruled out. If we do keep p_4 as an argument it is only to distinguish the p_4 -unaveraged structure functions obtained after the temporal gauge has been fixed from the p_4 -averaged ones which describe the static functions obtained for a fixed time slice.

C. Full vs. static propagator and their renormalization

Due to the energy independence of the dressing functions Eq. (20) we can average them over p_4 to minimize statistical fluctuations. The full propagator thus reads

$$S^{-1}(p) = i\mathbf{k}aA_s(|\mathbf{p}|) + i\mathbf{k}_4aA_t(|\mathbf{p}|) + B_m(|\mathbf{p}|), \quad (22)$$

while its static counterpart is, up to a constant proportional to the time extent of the lattice (see Appendix C):

$$S^{-1}(\mathbf{p}) = i\mathbf{k}aA_s(|\mathbf{p}|) + B_m(|\mathbf{p}|). \quad (23)$$

Alternatively, the static propagator can be taken at a fixed time slice, which is equivalent to averaging over all time slices without residual gauge fixing. As shown in Fig. 5a, A_t identically vanishes in this case and we again obtain Eq. (23). Such fixed time definition would of course make the static quark propagator much easier to calculate on lattices with large temporal extension, since for $L^3 \times T$ the inversion of the Dirac operator can be restricted to the L^3 spatial sub-lattice. Even if the procedure is repeated T times to improve the statistics one will still cut both CPU time and memory requirements and avoid possible I/O inefficiencies. We are planning to implement such improvement in all future analysis; besides enabling us to increase the number of configurations, this should also allow us to invest more computer time in the quality of the gauge fixing, see discussion in Sec. II B. Of course, this does not apply to the full propagator of Eq. (22), which will still need the inversion of the whole Dirac operator to resolve A_t .

Let us now define the renormalized propagators. While from Eq. (23) a static propagator as in Eq. (14) immediately follows, an explicit p_4 dependence of the dressing functions would have made it very difficult to cast $S(p)$ to the form Eq. (18), with the scale dependence confined to the proportionality factor. Due to the trivial p_4 -dependence of Eq. (22), however, the full (non-static) quark propagator does indeed take the lattice equivalent

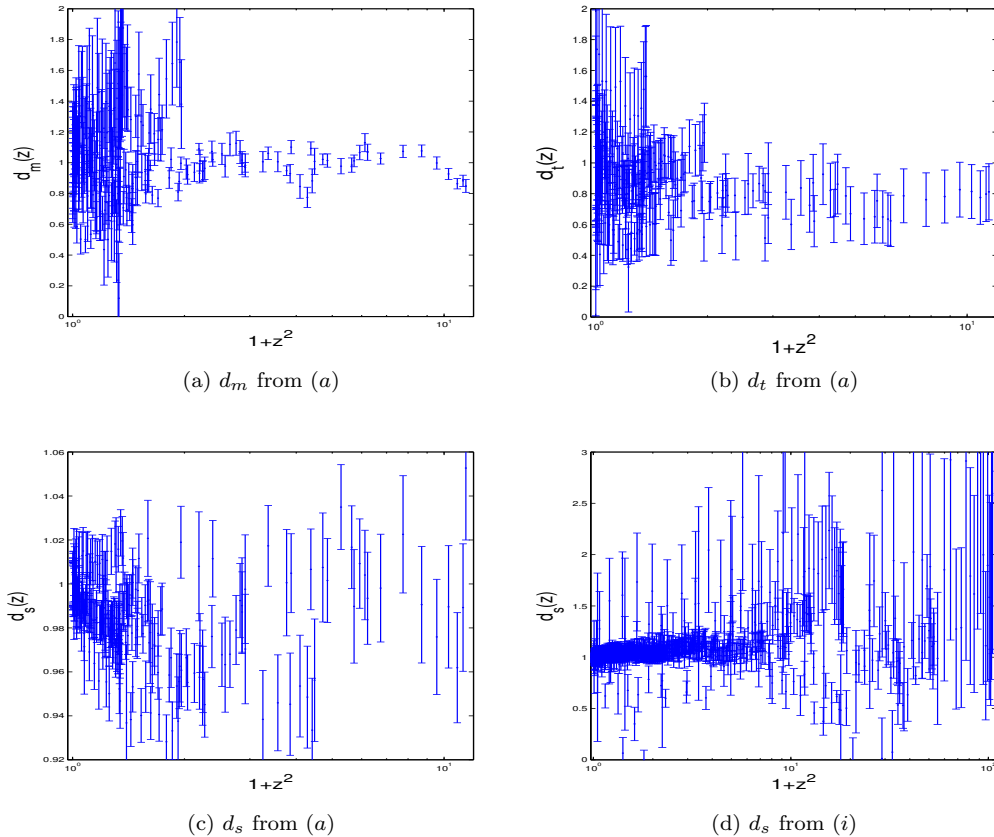


FIG. 2. Energy dependence of dressing functions as defined in Eq. (21).

form of Eq. (18):

$$S_\zeta(p) = \frac{Z_\zeta(|\mathbf{p}|)}{ia\mathbf{k} + ia\mathbf{k}_4\alpha(|\mathbf{p}|) + M(|\mathbf{p}|)}. \quad (24)$$

The renormalization function $Z_\zeta(|\mathbf{p}|)$, the mass function $M(|\mathbf{p}|)$ and the “energy form factor” $\alpha(|\mathbf{p}|)$ are derived in Appendix C:

$$\begin{aligned} Z_\zeta(|\mathbf{p}|) &= \left[\int_{-\pi}^{\pi} \frac{d\hat{p}_4}{2\pi} A_s(|\mathbf{p}|, p_4) \right]^{-1} \\ \alpha(|\mathbf{p}|) &= \frac{\int_{-\pi}^{\pi} \frac{d\hat{p}_4}{2\pi} A_t(|\mathbf{p}|, p_4)}{\int_{-\pi}^{\pi} \frac{d\hat{p}_4}{2\pi} A_s(|\mathbf{p}|, p_4)} \\ M(|\mathbf{p}|) &= \frac{\int_{-\pi}^{\pi} \frac{d\hat{p}_4}{2\pi} B_m(|\mathbf{p}|, p_4)}{\int_{-\pi}^{\pi} \frac{d\hat{p}_4}{2\pi} A_s(|\mathbf{p}|, p_4)} \end{aligned} \quad (25)$$

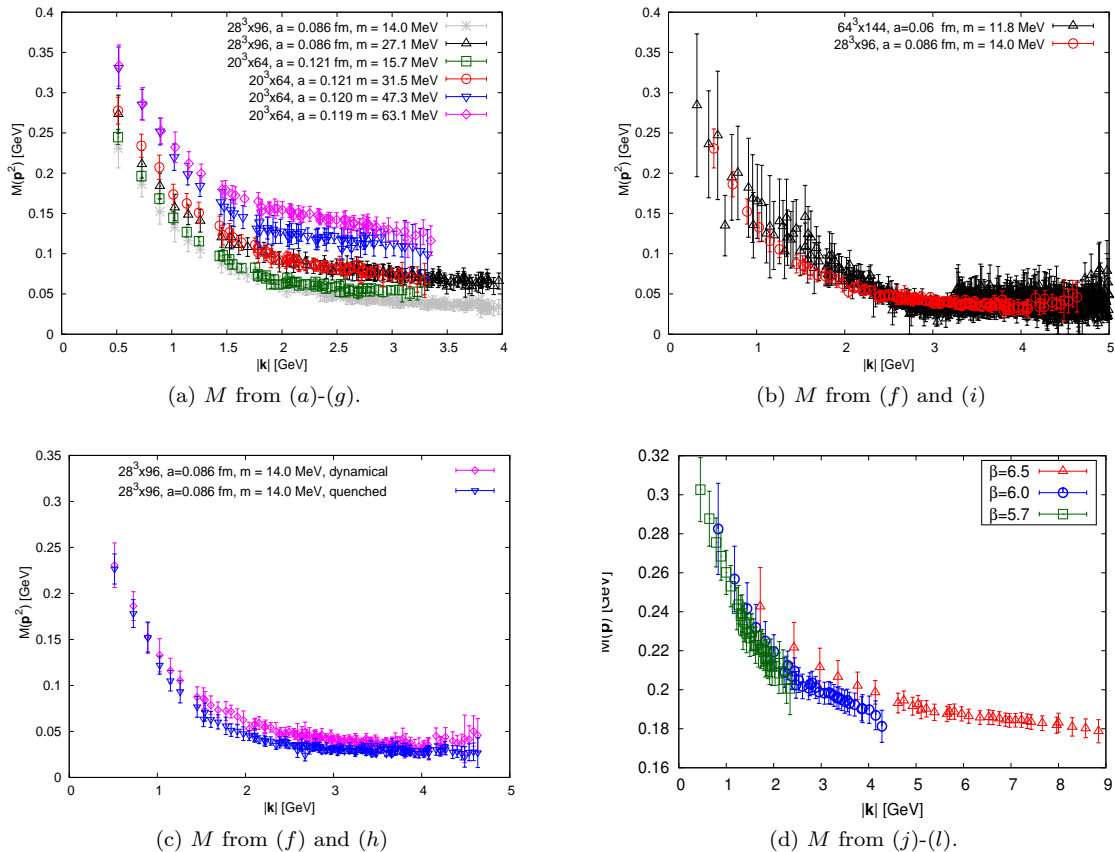
where the integrals here simply indicate a statistical average over the energy, given the p_4 independence of the dressing functions A ’s and B discussed in Sec. IV B.

To check renormalizability we now need to establish the scale invariance of $M(|\mathbf{p}|)$, $\alpha(|\mathbf{p}|)$ and study the scaling properties of $Z_\zeta(|\mathbf{p}|)$. Notice that M and Z_ζ can also be extracted from the equal-times propagator (cf. Eq. (14)), while α always requires the full p_4 -dependent propagator (cf. Eq. (24)).

In Fig. 3a we show the mass function $M(|\mathbf{p}|)$ from configuration sets (a)–(d), with scale $a \approx 0.12$ fm, compared to configuration sets (f) and (g), which have a scale $a = 0.086$ fm. These sets are chosen to have approximately the same physical volume, so as to minimize finite size effects at the two different cutoffs. As can be seen $M(|\mathbf{p}|)$ nicely agrees for the sets with similar masses, namely (a) (15.7 MeV) and (f) (14.0 MeV) on one side and (b) (31.5 MeV) and (g) (27.1 MeV) on the other side. We compare thus in Fig. 4b the corresponding wavefunction renormalization functions $Z_\zeta(|\mathbf{p}|)$ from configuration sets (g) and (b), finding a good agreement once we normalize both to $Z_\zeta(\zeta) = 1$ for the scale $\zeta = 3.0$ GeV. The scaling of the Landau gauge quark propagator was checked on the same lattices in Ref. [32], giving very similar results.

In Figs. 3b and 4c we compare $M(|\mathbf{p}|)$ and $Z_\zeta(|\mathbf{p}|)$ from configuration sets (f) (14.0 MeV) and (i) (11.9 MeV). Although on the latter we have less statistics and could only calculate Kogut–Susskind fermions, the agreement is still quite good.

We can thus conclude that the static propagator Eq. (14) is multiplicatively renormalizable. It should be stressed, however, that the wave function normalization Z_ζ (and α , cf. next paragraph) show satisfactory scaling

FIG. 3. Scaling of the mass function M

only when the improved Asqtad action is taken. This is in contrast to the running mass $M(|\mathbf{p}|)$, which is very robust against lattice artifacts, cf. e.g. Fig. 3d, where the unimproved Wilson action already gives a reasonable result ($m = 212$ MeV for all three data sets). A similar effect was also noticed in Landau gauge [32, 34–37].

Turning now to the full propagator Eq. (18), Figs. 5b–5c show the function α , i.e. the ratio of A_t to A_s , for different configuration sets. The scaling behaviour is very good both for the dynamical configurations Fig. 5b and for the quenched configurations Fig. 5c. We can thus conclude that the full (p_4 -dependent) propagator Eq. (18) is also multiplicatively renormalizable. As argued above, this fact allows us to define a dispersion relation for a single pseudo-quark as in Eq. (19).

Interestingly, Z_ζ turns out to be much more suppressed in the IR than its Landau gauge counterpart, cf. Fig. 6b, while α has a mild momentum dependence. The resulting dispersion relation $\omega_F(|\mathbf{p}|)$ is then found to be *IR enhanced*, as can be seen in Fig. 5d for sets (d)–(e), for which we have the best signal to noise ratio. If Z_ζ^2/α should indeed prove to vanish in the IR according to a power law,

$$Z_\zeta^2(|\mathbf{p}|)/\alpha(|\mathbf{p}|) \propto |\mathbf{p}|^k$$

we would find for the quark dispersion relation a behaviour similar to the Gribov formula for the gluon

[7, 13, 14]: in the ultraviolet $\omega_F \propto |\mathbf{p}|$ and in the infrared a power law $\omega_F \propto |\mathbf{p}|^{-k}$. The last relation describes an infrared diverging effective (pseudo-)energy for the quark, which would extend the Gribov-Zwanziger confinement scenario to the fermionic sector of QCD. With our present data we find a behaviour compatible with an infrared exponent of $k \approx 0.25$, but of course a reliable estimate would need better statistics on larger volumes, which we plan to collect in the near future. Notice also that the minimum of $\omega_F(|\mathbf{p}|)$ is around $|\mathbf{k}| \simeq 1.2$ GeV, which is compatible with the $a_t \rightarrow 0$ extrapolation of the gluonic Gribov mass [16] and the estimate of Λ we will extract in Sec. IV F.

D. Effects of dynamical quarks

The dynamical and quenched configuration sets (f) and (h) have same size and scale. This makes them well suited to study quantitatively the effects of quenching. To this end we have calculated on both sets the Coulomb gauge quark propagator with equal bare mass, viz. the light sea quark mass of set (f). The resulting mass and renormalization functions $M(|\mathbf{p}|)$ and $Z_\zeta(|\mathbf{p}|)$ are compared in Figs. 3c and 4d. We find a slight screening of the dynamical mass generation in the case of full QCD,

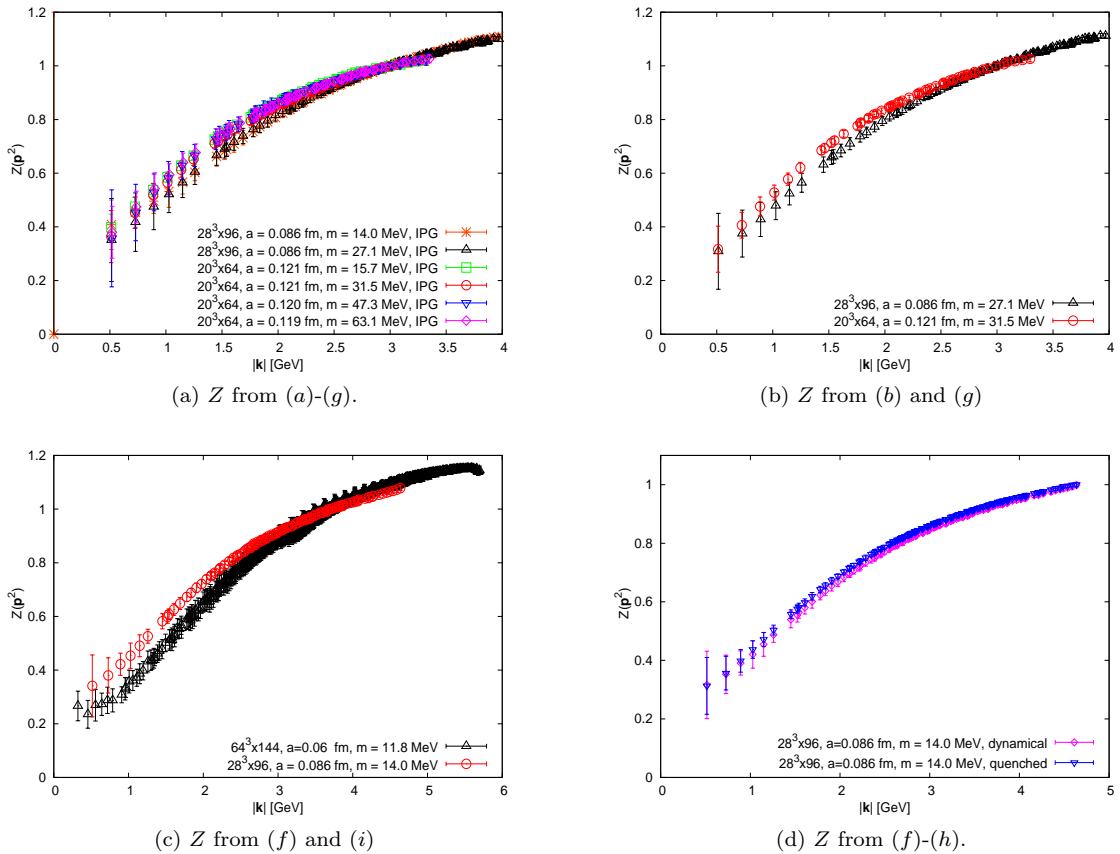


FIG. 4. Scaling function Z . The renormalization point ζ is set at 3 GeV in (4a) and (4b), 3.7 GeV in 4c and 4.64 GeV in 4d

similarly to what was seen in Landau gauge [37].

E. Comparison to Landau gauge

In Fig. 6a and 6b we show the comparison between the mass and renormalization function in Coulomb gauge, Eq. (14), and Landau gauge, Eq. (11). The data for the Landau case was taken from Ref. [32]. Up to slight differences in the intermediate and high momentum region, M is almost identical in both gauges, especially in the IR, while Z_ζ shows a much stronger gauge dependence. For this comparison, the renormalization point has been set at $\zeta = 4.64$ GeV. These findings nicely agree with the discussion in Sec. III B.

F. Chiral limit

For the configuration sets (a)–(d) the dynamical masses decrease at constant cutoff. We have therefore attempted a chiral extrapolation of the mass function determined for these sets with Asqtad fermions at the dynamical point. This procedure should minimize systematic errors due to partial quenching. The result is shown

in Fig. 6c. In addition, we have also made a chiral extrapolation of the set (i) using Kogut-Susskind fermions (Fig. 6d), where the mass has been fixed to five different values, with only the last at the dynamical point. The result of the latter, although quite noisy in the IR, allows us to extend the momentum range and extract further information in the UV. Within error bars the two chiral extrapolations agree, cf. Fig. 7a. We find that all data can be well described by a function of the form:

$$M(|\mathbf{k}|, m_b) = \frac{m_\chi(m_b)}{1 + b \frac{|\mathbf{k}|^2}{\Lambda^2} \log \left(e + \frac{|\mathbf{k}|^2}{\Lambda^2} \right)^{-\gamma}} + \frac{m_r(m_b)}{\log \left(e + \frac{|\mathbf{k}|^2}{\Lambda^2} \right)^\gamma} \quad (26)$$

where b is a constant, γ is the anomalous dimension and Λ is the QCD scale. In this fit we have also defined a renormalized Coulomb dressed mass m_r and a chiral quark mass, both of which depend on the bare mass m_b . Performing a simultaneous fit for all data we find $b = 2.9(1)$, $\gamma = 0.84(2)$ and $\Lambda = 1.22(6)$ GeV with $\chi^2/\text{d.o.f.} = 1.06$. For the extrapolated data of Fig. 7a we further find (constraining $m_r \equiv 0$) $m_\chi = 0.31(1)$ GeV, in very good agreement with the constituent mass expected from quark models. In Fig. 7b we show the dependence of m_χ on the bare mass m_b . For bare masses larger than $m_b \simeq$

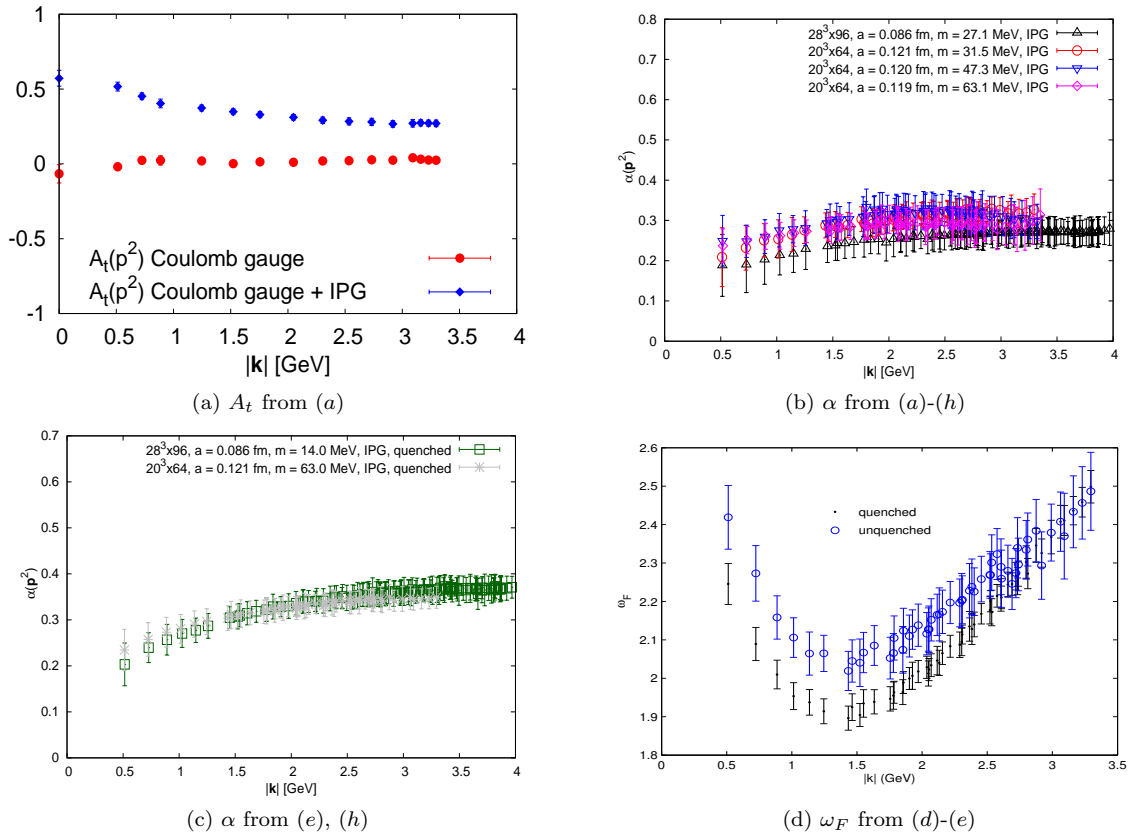


FIG. 5. Scaling of the temporal function α ; ω_F as in Eq. (19).

100 MeV the chiral quark mass practically disappears; on the other hand we find that the Coulomb gauge dressed mass m_r increases more than linearly with m_b , cf. Fig 7c. One should not however over-interpret such result, since the splitting between the two masses in the intermediate region will strongly depend on the fit function chosen. A more reliable extraction of m_r will need to be based on data at smaller lattice spacing, pushing the fits in the higher UV region. Finally, Fig. 7d displays the total constituent IR mass $M(0) = m_\chi + m_r$ from Eq.(26) as a function of m_b ; this should turn out to be fit independent as soon as the available data will push far enough in the IR region.

Similar calculations with Asqtad fermions at the finest spaced lattice and with the largest overall volume are currently under way to confirm our results.

V. CONCLUSIONS

In this paper we have studied the static and full quark propagator in Coulomb gauge. We have shown that, for improved actions minimizing discretization errors, $S(p)$ has a trivial energy dependence and therefore both $S(p)$ and the equal-time propagator $S(|p|)$ are multiplicatively renormalizable. The mass function entering both propagators agrees semi-quantitatively with its Landau gauge

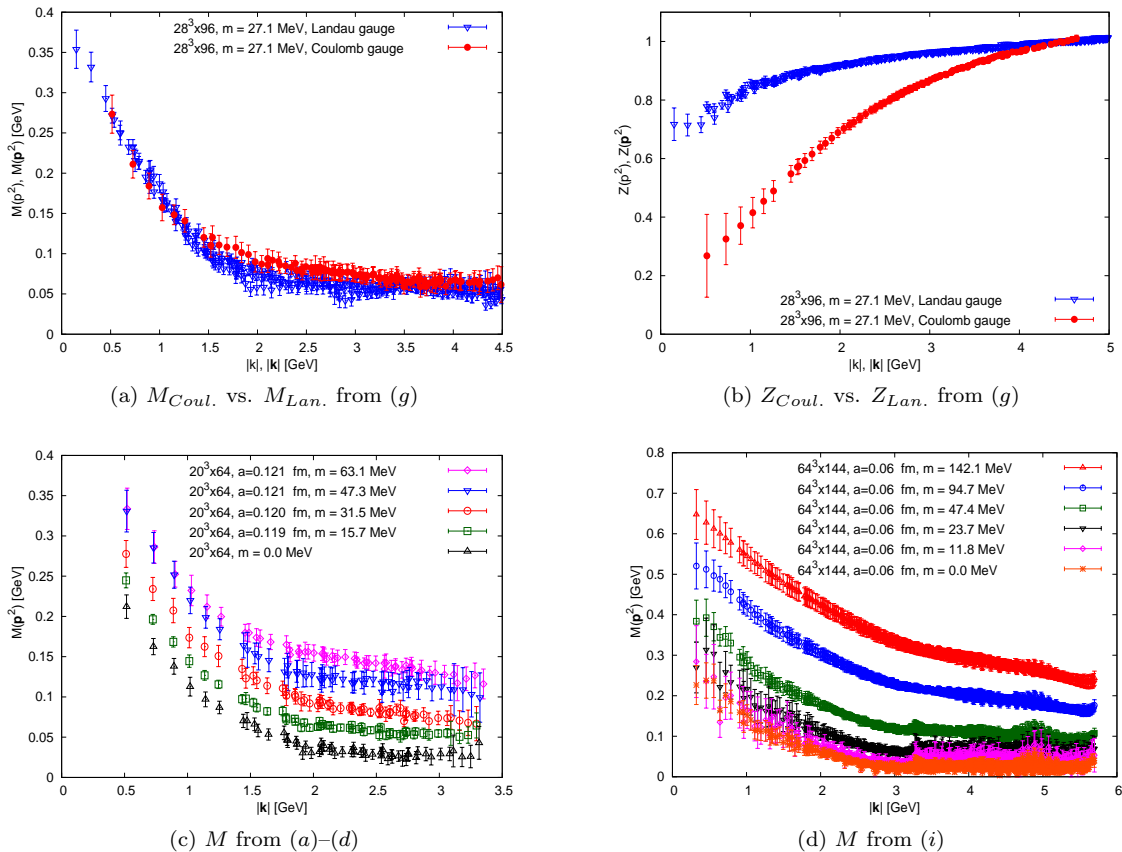
counterpart. However, for future work, it will allow for a more efficient determination of the chiral parameters, the constituent quark masses and the quark anomalous dimension, since as we have shown the Dirac operator in Coulomb gauge is energy independent and its static version, which holds all information about the running mass and the wave function renormalization, can be inverted at each fixed time slice.

Moreover, the full (non-static) Coulomb propagator gives access to an effective energy for the quark field. With our current data, the dispersion relation is compatible with a Gribov kind of behaviour. Quark confinement could thus be explained in this picture by a diverging IR effective energy, which is a first evidence that the Gribov-Zwanziger confinement scenario could be extended to the fermionic sector of QCD.

ACKNOWLEDGMENTS

We wish to thank P. O. Bowman for giving us access to the Landau gauge data used in Sec. IV E and for careful reading of the manuscript.

This work was partially supported by DFG grant Re864/6-3; M.S. is supported by the Research Executive Agency (REA) of the European Union under Grant Agreement PITN-GA-2009-238353 (ITN STRONGnet).

FIG. 6. Landau vs. Coulomb gauge (top); chiral behaviour of M (bottom)

Appendix A: Fixing the residual gauge

After fixing the Coulomb gauge at each time-slice x_4 we are still left with the freedom to perform a global gauge transformation $g(x_4)$ at each x_4 . To determine it we implement the lattice equivalent to the residual continuum condition (7). Let us begin by averaging, for every fixed time-slice x_4 , over the spatial coordinates \mathbf{x} in $U_4(x)$,

$$\hat{u}(x_4) \equiv \frac{1}{L^3} \sum_{\mathbf{x}} U_4(x). \quad (\text{A1})$$

Next we project the matrix $\hat{u}(x_4)$ back to $SU(3)$ by Cabibbo–Marinari cooling [53], i.e. we look for a $u(x_4) \in SU(3)$ satisfying:

$$\max_{u(x_4)} \Re \text{tr} [u(x_4) \hat{u}^\dagger(x_4)]. \quad (\text{A2})$$

Although such projection is not unique, we believe it to be a “natural” choice; of course, different projections will lead to different temporal gauges. However, since all dressing functions in S turn out to be energy independent, the choice of a different prescription should eventually not influence the results.

We now seek a gauge transformation $g(x_4)$ such that

$$u(x_4) \xrightarrow{!} \text{const.} \quad (\text{A3})$$

This can be achieved defining the integrated Polyakov loop:

$$P \equiv \text{tr} \left[\prod_{x_4} u(x_4) \right] \quad (\text{A4})$$

and choosing $g(x_4)$ such that for all x_4

$$g(x_4) u(x_4) g^\dagger(x_4 + 1) = P^{1/T}, \quad (\text{A5})$$

where T is the temporal extension of the lattice and $P^{1/T}$ is the T -th root of P . To do so we (arbitrarily) choose $g(0) = \mathbf{1}$ and then determine all $g(x_4)$ recursively,

$$g^\dagger(x_4 + 1) = u^\dagger(x_4) g^\dagger(x_4) P^{1/T}. \quad (\text{A6})$$

If we now gauge all links via the transformation $g(x_4)$ we have

$$U'_4(\mathbf{x}, x_4) = g(x_4) U_4(\mathbf{x}, x_4) g^\dagger(x_4 + 1) \quad (\text{A7})$$

$$U'_i(\mathbf{x}, x_4) = g(x_4) U_i(\mathbf{x}, x_4) g^\dagger(x_4), \quad (\text{A8})$$

respectively. The new temporal links U'_4 obey Eq. (A3); if $u \sim \hat{u}$ as in the case of $SU(2)$, this condition would via Eq. (A1) translate into $\partial_4 \sum_{\mathbf{x}} U'_4(x)$, which is the equivalent to the continuum condition (7). For $G = SU(3)$, however, the sum of colour matrices is not proportional to

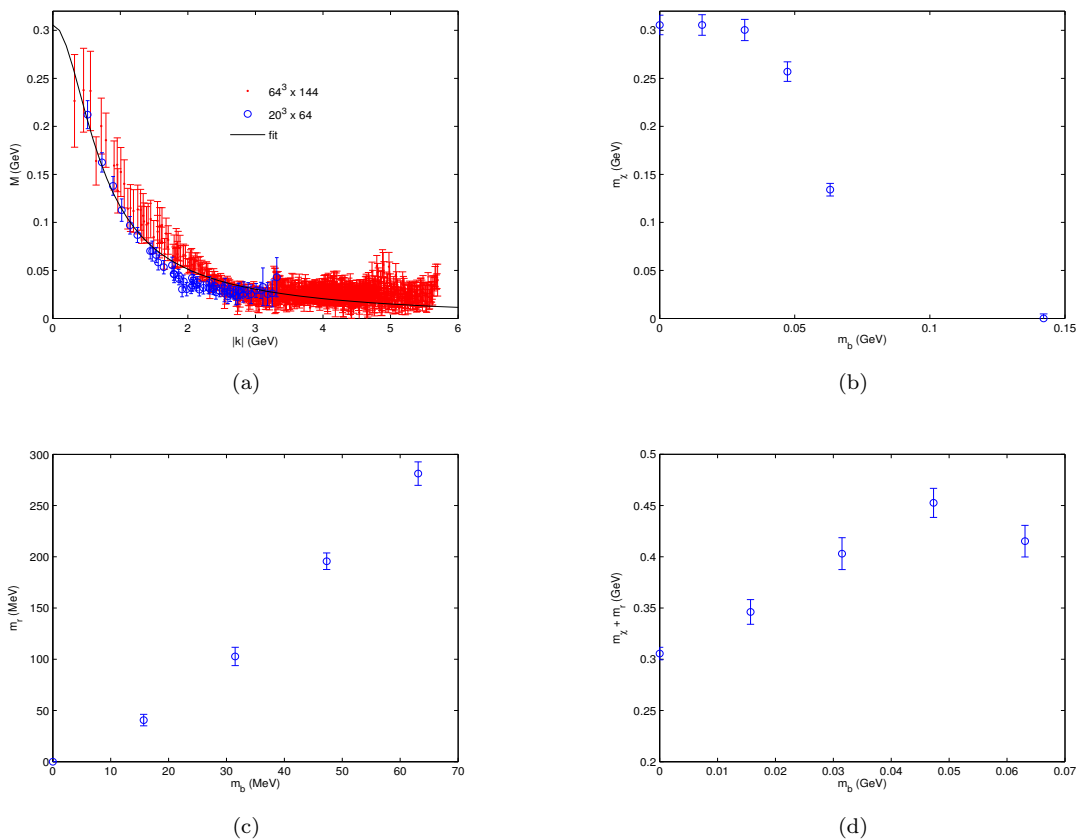


FIG. 7. The chiral limit taken from the dynamical point of configuration sets (a)–(d), compared to the chiral limit from set (i) (partially quenched) and to the fit to Eq. (26).

an $SU(3)$ matrix, and we can only choose $\hat{u}(x_4)$ as close as possible to $u(x_4)$. The cooling step Eq. (A2) implements thus the continuum condition Eq. (7) as much as possible for the color group $G = SU(3)$. From Eq. (A8), we also see that the new transformation $g(x_4)$ acts as a global gauge transformation at each fixed time slice x_4 , i.e. the Coulomb gauge condition remains unaffected.

Appendix B: Staggered quark propagators

We extend here to Coulomb gauge the decomposition of the staggered quark propagator in Landau gauge performed in [37, 54]. The Kogut–Susskind propagator reads at tree-level:

$$S_{\alpha\beta}^{(0)}(q)^{-1} = i \sum_{\mu} (\bar{\gamma}_{\mu})_{\alpha\beta} \sin(\hat{q}_{\mu}) + \hat{m}_0 \bar{\delta}_{\alpha\beta} \quad (\text{B1})$$

where α, β are staggered multi-indices, $\alpha = (\alpha_1, \dots, \alpha_4)$, $\alpha_{\mu} \in \{0, 1\}$, while $\bar{\delta}_{\alpha\beta} \equiv \prod_{\mu} \delta_{\alpha_{\mu}\beta_{\mu} \bmod 2}$ and

$$(\bar{\gamma}_{\mu})_{\alpha\beta} \equiv (-1)^{\alpha_{\mu}} \bar{\delta}_{\alpha+\theta(\mu),\beta}, \quad (\text{B2})$$

where the ν^{th} component of the 4-vectors $\theta(\mu)$ is given by:

$$\theta_{\nu}(\mu) = \begin{cases} 1 & \text{if } \nu < \mu, \\ 0 & \text{else,} \end{cases} \quad (\text{B3})$$

giving the staggered Dirac algebra

$$\{\bar{\gamma}_{\mu}, \bar{\gamma}_{\nu}\}_{\alpha\beta} = 2\delta_{\mu\nu} \bar{\delta}_{\alpha\beta}. \quad (\text{B4})$$

The discrete momenta $\hat{q}_{\mu} \equiv aq_{\mu}$ are restricted for staggered fermions to the inner half of the Brillouin zone, $\hat{q}_{\mu} \in (-\frac{\pi}{2}, \frac{\pi}{2}]$, and are related to the ordinary lattice momenta $p_{\mu} \in (-\pi, \pi]$ via

$$\hat{p}_{\mu} = \hat{q}_{\mu} + \rho_{\mu}\pi, \quad \rho_{\mu} = \{0, 1\}. \quad (\text{B5})$$

In the following we will use the common abbreviation $\hat{k}_{\mu} \equiv \sin \hat{q}_{\mu}$.

Summing over one of the propagator's multi-indices, $\sum_{\beta} = \sum_{\beta_1, \dots, \beta_4=0}^1$, we define

$$G_{\alpha}^{(0)}(q) \equiv \sum_{\beta} S_{\alpha\beta}^{(0)}(q) = \sum_{\beta} \frac{-i(\bar{\gamma}_{\mu})_{\alpha\beta} \hat{k}_{\mu} + \hat{m}_0 \bar{\delta}_{\alpha\beta}}{\hat{k}^2 + \hat{m}_0^2}. \quad (\text{B6})$$

In order to evaluate the r.h.s. of Eq. (B6), we note that

$$\sum_{\beta} (\bar{\gamma}_{\mu})_{\alpha\beta} \equiv \sum_{\beta} (-1)^{\alpha\mu} \bar{\delta}_{\alpha+\theta(\mu),\beta} = (-1)^{\alpha\mu}. \quad (\text{B7})$$

We now want to extract the dressing functions of the inverse Coulomb propagator:

$$G_{\alpha}^{-1}(q) \equiv i(-1)^{\alpha_i} \hat{k}_i a A_s(|\mathbf{q}|, q_4^2) + i(-1)^{\alpha_4} \hat{k}_4 a A_t(|\mathbf{q}|, q_4^2) \\ + i(-1)^{\alpha_i+\alpha_4} \hat{k}_i a A_d(|\mathbf{q}|, q_4^2) + B_m(|\mathbf{q}|, q_4^2). \quad (\text{B8})$$

On the other hand, we can also express the propagator in terms of new dressing functions \mathcal{A}_s , \mathcal{A}_t , \mathcal{A}_d and \mathcal{B}_m :

$$G_{\alpha}(q) \equiv -i(-1)^{\alpha_i} \hat{k}_i a \mathcal{A}_s(|\mathbf{q}|, q_4^2) - i(-1)^{\alpha_4} \hat{k}_4 a \mathcal{A}_t(|\mathbf{q}|, q_4^2) \\ - i(-1)^{\alpha_i+\alpha_4} \hat{k}_i a \mathcal{A}_d(|\mathbf{q}|, q_4^2) + \mathcal{B}_m(|\mathbf{q}|, q_4^2) \\ = [-i(-1)^{\alpha_i} \hat{k}_i a \mathcal{A}_s(|\mathbf{q}|, q_4^2) - i(-1)^{\alpha_4} \hat{k}_4 a \mathcal{A}_t(|\mathbf{q}|, q_4^2) \\ - i(-1)^{\alpha_i+\alpha_4} \hat{k}_i a \mathcal{A}_d(|\mathbf{q}|, q_4^2) + \mathcal{B}_m(|\mathbf{q}|, q_4^2)] / D^2(|\mathbf{q}|, q_4^2) \quad (\text{B9})$$

where we have defined

$$D^2(|\mathbf{q}|, q_4^2) \equiv \sum_i \hat{k}_i^2 a^2 A_s^2(|\mathbf{q}|, q_4^2) + \hat{k}_4^2 a^2 A_t^2(|\mathbf{q}|, q_4^2) \\ + \sum_i \hat{k}_i^2 a^2 A_d^2(|\mathbf{q}|, q_4^2) + B_m^2(|\mathbf{q}|, q_4^2). \quad (\text{B10})$$

After some algebra it can be shown that

$$D^2(|\mathbf{q}|, q_4^2) \mathcal{D}^2(|\mathbf{q}|, q_4^2) = 1 \quad (\text{B11})$$

where

$$\mathcal{D}^2(|\mathbf{q}|, q_4^2) \equiv \sum_i \hat{k}_i^2 a^2 \mathcal{A}_s^2(|\mathbf{q}|, q_4^2) + \hat{k}_4^2 a^2 \mathcal{A}_t^2(|\mathbf{q}|, q_4^2) \\ + \sum_i \hat{k}_i^2 a^2 \mathcal{A}_d^2(|\mathbf{q}|, q_4^2) + \mathcal{B}_m^2(|\mathbf{q}|, q_4^2). \quad (\text{B12})$$

Now we multiply Eq. (B9) by $(-1)^{\alpha_i}$, $(-1)^{\alpha_4}$, $(-1)^{\alpha_i+\alpha_4}$ or 1, respectively, and sum over α using

$$\sum_{\alpha} (-1)^{\alpha\mu+\alpha\nu} = 16 \delta_{\mu\nu}. \quad (\text{B13})$$

Taking finally the trace with respect to color indices we obtain:

$$\mathcal{A}_s(|\mathbf{q}|, q_4^2) \equiv \frac{A_s(|\mathbf{q}|, q_4^2)}{D^2(|\mathbf{q}|, q_4^2)} = \frac{i}{16N_c \sum_i \hat{k}_i^2 a} \\ \times \sum_i \sum_{\alpha} (-1)^{\alpha_i} \hat{k}_i \text{tr} [G_{\alpha}(q)], \quad (\text{B14})$$

$$\mathcal{A}_t(|\mathbf{q}|, q_4^2) \equiv \frac{A_t(|\mathbf{q}|, q_4^2)}{D^2(|\mathbf{q}|, q_4^2)} = \frac{i}{16N_c \hat{k}_4^2 a} \\ \times \sum_{\alpha} (-1)^{\alpha_4} \hat{k}_4 \text{tr} [G_{\alpha}(q)], \quad (\text{B15})$$

$$\mathcal{A}_d(|\mathbf{q}|, q_4^2) \equiv \frac{A_d(|\mathbf{q}|, q_4^2)}{D^2(|\mathbf{q}|, q_4^2)} = \frac{i}{16N_c \sum_i \hat{k}_i^2 a} \\ \times \sum_i \sum_{\alpha} (-1)^{\alpha_i+\alpha_4} \hat{k}_i \text{tr} [G_{\alpha}(q)], \quad (\text{B16})$$

$$\mathcal{B}_m(|\mathbf{q}|, q_4^2) \equiv \frac{B_m(|\mathbf{q}|, q_4^2)}{D^2(|\mathbf{q}|, q_4^2)} = \frac{1}{16N_c} \sum_{\alpha} \text{tr} [G_{\alpha}(q)]. \quad (\text{B17})$$

From Eq. (B11) and Eqs. (B14-B17) we can now easily extract the dressing functions A_s , A_t , A_d and B_m .

Turning next to Asqtad improved fermions, their tree-level propagator reads:

$$S_{\alpha\beta}^{(0)}(q)^{-1} = iu_0 \sum_{\mu} (\bar{\gamma}_{\mu})_{\alpha\beta} \sin(\hat{q}_{\mu}) \\ \times \left[1 + \frac{1}{6} \sin^2(\hat{q}_{\mu}) \right] + \hat{m} \bar{\delta}_{\alpha\beta} \quad (\text{B18})$$

and the decomposition given above can be performed in essentially the same way. We only have to keep in mind, though, that the dressing functions will also get contributions from the tadpole factors u_0 , which have to be eliminated a posteriori.

Appendix C: Formulas for Z , M and α

To extract $Z(|\mathbf{p}|)$, $M(|\mathbf{p}|)$ and α we can proceed as in Appendix B. Recalling that $A_d \equiv 0$ we write the propagator as ($k_{\mu} \equiv \sin p_{\mu}$):

$$S^{-1}(p) = i\hat{k}a A_s(|\mathbf{p}|, p_4) + i\hat{k}_4 a A_t(|\mathbf{p}|, p_4) + B_m(|\mathbf{p}|, p_4) \quad (\text{C1})$$

$$= i\hat{k}a \frac{\mathcal{A}_s(|\mathbf{p}|, p_4)}{\mathcal{D}^2(|\mathbf{p}|, p_4)} + i\hat{k}_4 a \frac{\mathcal{A}_t(|\mathbf{p}|, p_4)}{\mathcal{D}^2(|\mathbf{p}|, p_4)} + \frac{B_m(|\mathbf{p}|, p_4)}{\mathcal{D}^2(|\mathbf{p}|, p_4)} \quad (\text{C2})$$

and

$$S(p) = -i\hat{k}a \mathcal{A}_s(|\mathbf{p}|, p_4) - i\hat{k}_4 a \mathcal{A}_t(|\mathbf{p}|, p_4) + B_m(|\mathbf{p}|, p_4) \quad (\text{C3})$$

$$= -i\hat{k}a \frac{A_s(|\mathbf{p}|, p_4)}{D^2(|\mathbf{p}|, p_4)} - i\hat{k}_4 a \frac{A_t(|\mathbf{p}|, p_4)}{D^2(|\mathbf{p}|, p_4)} + \frac{B_m(|\mathbf{p}|, p_4)}{D^2(|\mathbf{p}|, p_4)}. \quad (\text{C4})$$

Here the denominators are

$$D^2(|\mathbf{p}|, p_4) \equiv \mathbf{k}^2 a^2 A_s^2(|\mathbf{p}|, p_4) + k_4^2 a^2 A_t^2(|\mathbf{p}|, p_4) \\ + B_m^2(|\mathbf{p}|, p_4), \quad (\text{C5})$$

$$\mathcal{D}^2(|\mathbf{p}|, p_4) \equiv \mathbf{k}^2 a^2 \mathcal{A}_s^2(|\mathbf{p}|, p_4) + k_4^2 a^2 \mathcal{A}_t^2(|\mathbf{p}|, p_4) \\ + \mathcal{B}_m^2(|\mathbf{p}|, p_4), \quad (\text{C6})$$

and they still obey

$$D^2(|\mathbf{p}|, p_4^2) \mathcal{D}^2(|\mathbf{p}|, p_4^2) = 1. \quad (\text{C7})$$

This looks just like the Landau gauge case, but with an extra structure function. Applying the same line of reasoning as in Ref. [37, 54] now leads immediately to Eq. (25) in the main text.

Turning now to the static propagators, we first note that $A_t(|\mathbf{p}|, p_4)$ is an even function of p_4 , so that the γ_4 contribution cancels by T -symmetry when integrating $S^{-1}(p)$ over the (energy) Brillouin zone. Therefore:

$$S^{-1}(\mathbf{p}) = i\mathbf{k}a \int_{-\pi}^{\pi} \frac{d\hat{p}_4}{2\pi} A_s(|\mathbf{p}|, p_4) + \int_{-\pi}^{\pi} \frac{d\hat{p}_4}{2\pi} B_m(|\mathbf{p}|, p_4) \quad (\text{C8})$$

$$= i\mathbf{k}a \int_{-\pi}^{\pi} \frac{d\hat{p}_4}{2\pi} \frac{A_s(|\mathbf{p}|, p_4)}{D^2(|\mathbf{p}|, p_4)} + \int_{-\pi}^{\pi} \frac{d\hat{p}_4}{2\pi} \frac{B_m(|\mathbf{p}|, p_4)}{D^2(|\mathbf{p}|, p_4)} \quad (\text{C9})$$

and

$$S(\mathbf{p}) = -i\mathbf{k}a \int_{-\pi}^{\pi} \frac{d\hat{p}_4}{2\pi} A_s(|\mathbf{p}|, p_4) + \int_{-\pi}^{\pi} \frac{d\hat{p}_4}{2\pi} B_m(|\mathbf{p}|, p_4) \quad (\text{C10})$$

$$= -i\mathbf{k}a \int_{-\pi}^{\pi} \frac{d\hat{p}_4}{2\pi} \frac{A_s(|\mathbf{p}|, p_4)}{D^2(|\mathbf{p}|, p_4)} + \int_{-\pi}^{\pi} \frac{d\hat{p}_4}{2\pi} \frac{B_m(|\mathbf{p}|, p_4)}{D^2(|\mathbf{p}|, p_4)}. \quad (\text{C11})$$

From Eq. (C8) we obtain:

$$S(\mathbf{p}) = \frac{-i\mathbf{k}a \int_{-\pi}^{\pi} \frac{d\hat{p}_4}{2\pi} A_s(|\mathbf{p}|, p_4) + \int_{-\pi}^{\pi} \frac{d\hat{p}_4}{2\pi} B_m(|\mathbf{p}|, p_4)}{P^2(|\mathbf{p}|)}, \quad (\text{C12})$$

$$P^2(|\mathbf{p}|) \equiv \mathbf{k}^2 a^2 \left(\int_{-\pi}^{\pi} \frac{d\hat{p}_4}{2\pi} A_s(|\mathbf{p}|, p_4) \right)^2 + \left(\int_{-\pi}^{\pi} \frac{d\hat{p}_4}{2\pi} B_m(|\mathbf{p}|, p_4) \right)^2, \quad (\text{C13})$$

while inverting Eq. (C10) yields:

$$S^{-1}(\mathbf{p}) = \frac{i\mathbf{k}a \int_{-\pi}^{\pi} \frac{d\hat{p}_4}{2\pi} A_s(|\mathbf{p}|, p_4) + \int_{-\pi}^{\pi} \frac{d\hat{p}_4}{2\pi} B_m(|\mathbf{p}|, p_4)}{P^2(|\mathbf{p}|)}, \quad (\text{C14})$$

$$P^2(|\mathbf{p}|) \equiv \mathbf{k}^2 a^2 \left(\int_{-\pi}^{\pi} \frac{d\hat{p}_4}{2\pi} A_s(|\mathbf{p}|, p_4) \right)^2 + \left(\int_{-\pi}^{\pi} \frac{d\hat{p}_4}{2\pi} B_m(|\mathbf{p}|, p_4) \right)^2. \quad (\text{C15})$$

From Eq. (C8) and Eq. (C14) we thus obtain:

$$\int_{-\pi}^{\pi} \frac{d\hat{p}_4}{2\pi} A_s(|\mathbf{p}|, p_4) = \frac{\int_{-\pi}^{\pi} \frac{d\hat{p}_4}{2\pi} A_s(|\mathbf{p}|, p_4)}{P^2(|\mathbf{p}|)}, \quad (\text{C16})$$

$$\int_{-\pi}^{\pi} \frac{d\hat{p}_4}{2\pi} B_m(|\mathbf{p}|, p_4) = \frac{\int_{-\pi}^{\pi} \frac{d\hat{p}_4}{2\pi} B_m(|\mathbf{p}|, p_4)}{P^2(|\mathbf{p}|)} \quad (\text{C17})$$

while Eq. (C10) and Eq. (C12) give:

$$\int_{-\pi}^{\pi} \frac{d\hat{p}_4}{2\pi} A_s(|\mathbf{p}|, p_4) = \frac{\int_{-\pi}^{\pi} \frac{d\hat{p}_4}{2\pi} A_s(|\mathbf{p}|, p_4)}{P^2(|\mathbf{p}|)}, \quad (\text{C18})$$

$$\int_{-\pi}^{\pi} \frac{d\hat{p}_4}{2\pi} B_m(|\mathbf{p}|, p_4) = \frac{\int_{-\pi}^{\pi} \frac{d\hat{p}_4}{2\pi} B_m(|\mathbf{p}|, p_4)}{P^2(|\mathbf{p}|)}. \quad (\text{C19})$$

Writing the static propagator as:

$$S(\mathbf{p}) = Z(|\mathbf{p}|) \frac{-i\mathbf{k}a + M(|\mathbf{p}|)}{\mathbf{k}^2 a^2 + M^2(|\mathbf{p}|)}, \quad (\text{C20})$$

$$S^{-1}(\mathbf{p}) = Z^{-1}(|\mathbf{p}|) (i\mathbf{k}a + M(|\mathbf{p}|)). \quad (\text{C21})$$

and comparing Eq. (C14) and Eq. (C21) we finally have:

$$Z(|\mathbf{p}|) = \frac{P^2(|\mathbf{p}|)}{\int_{-\pi}^{\pi} \frac{d\hat{p}_4}{2\pi} A_s(|\mathbf{p}|, p_4)} = \frac{1}{\int_{-\pi}^{\pi} \frac{d\hat{p}_4}{2\pi} A_s(|\mathbf{p}|, p_4)}, \quad (\text{C22})$$

$$M(|\mathbf{p}|) = \frac{\int_{-\pi}^{\pi} \frac{d\hat{p}_4}{2\pi} B_m(|\mathbf{p}|, p_4)}{\int_{-\pi}^{\pi} \frac{d\hat{p}_4}{2\pi} A_s(|\mathbf{p}|, p_4)} = \frac{\int_{-\pi}^{\pi} \frac{d\hat{p}_4}{2\pi} B_m(|\mathbf{p}|, p_4)}{\int_{-\pi}^{\pi} \frac{d\hat{p}_4}{2\pi} A_s(|\mathbf{p}|, p_4)}. \quad (\text{C23})$$

-
- [1] A. P. Szczepaniak and E. S. Swanson, Phys. Rev., **D65**, 025012 (2002), arXiv:hep-ph/0107078.
[2] C. Feuchter and H. Reinhardt, Phys. Rev., **D70**, 105021 (2004), arXiv:hep-th/0408236.
[3] C. Feuchter and H. Reinhardt, (2004), arXiv:hep-th/0402106 [hep-th].
[4] N. Christ and T. Lee, Phys.Rev., **D22**, 939 (1980).
[5] G. Burgio, R. De Pietri, H. A. Morales-Tecotl, L. F. Urrutia, and J. D. Vergara, Nucl. Phys., **B566**, 547 (2000), arXiv:hep-lat/9906036.
[6] D. Epple, H. Reinhardt, and W. Schleifenbaum, Phys. Rev., **D75**, 045011 (2007), arXiv:hep-th/0612241.
[7] V. N. Gribov, Nucl. Phys., **B139**, 1 (1978).
[8] D. Zwanziger, Nucl.Phys., **B412**, 657 (1994).

- [9] D. Zwanziger, Nucl. Phys., **B485**, 185 (1997), arXiv:hep-th/9603203.
[10] H. Reinhardt, Phys. Rev. Lett., **101**, 061602 (2008), arXiv:0803.0504 [hep-th].
[11] M. Quandt, H. Reinhardt, and G. Burgio, Phys.Rev., **D81**, 065016 (2010), arXiv:1001.3699 [hep-lat].
[12] H. Reinhardt, M. Quandt, and G. Burgio, Phys. Rev. D, **85**, 025001 (2012), arXiv:1110.2927 [hep-th].
[13] G. Burgio, M. Quandt, and H. Reinhardt, Phys. Rev. Lett., **102**, 032002 (2009), arXiv:0807.3291 [hep-lat].
[14] G. Burgio, M. Quandt, and H. Reinhardt, PoS, **CONFINEMENT8**, 051 (2008), arXiv:0812.3786 [hep-lat].
[15] G. Burgio, M. Quandt, and H. Reinhardt, Phys.Rev., **D81**, 074502 (2010), arXiv:0911.5101 [hep-lat].

- [16] G. Burgio, M. Quandt, and H. Reinhardt, (2012), arXiv:1205.5674 [hep-lat].
- [17] M. Pak and H. Reinhardt, *Physics Letters B*, **707**, 566 (2012), arXiv:1107.5263 [hep-ph].
- [18] G. Burgio and al. (TrinLat), *Phys. Rev.*, **D67**, 114502 (2003), arXiv:hep-lat/0303005.
- [19] P. Watson and H. Reinhardt, *Phys. Rev.*, **D76**, 125016 (2007), arXiv:0709.0140 [hep-th].
- [20] H. Reinhardt and P. Watson, *Phys. Rev.*, **D79**, 045013 (2009), arXiv:0808.2436 [hep-th].
- [21] A. Andrasi and J. C. Taylor, *Annals Phys.*, **326**, 1053 (2011), arXiv:1010.5911 [hep-th].
- [22] C. W. Bernard, T. Burch, K. Orginos, D. Toussaint, T. A. DeGrand, *et al.*, *Phys.Rev.*, **D64**, 054506 (2001), arXiv:hep-lat/0104002 [hep-lat].
- [23] C. Aubin, C. Bernard, C. DeTar, J. Osborn, S. Gottlieb, *et al.*, *Phys.Rev.*, **D70**, 094505 (2004), arXiv:hep-lat/0402030 [hep-lat].
- [24] M. Di Pierro, J. Hetrick, S. Cholia, and D. Skinner, *PoS, LATTICE2011*, 305 (2011), arXiv:1112.2193 [hep-lat].
- [25] M. Di Pierro *et al.* (FermiQCD Collaboration), *Nucl.Phys.Proc.Suppl.*, **129**, 832 (2004), arXiv:hep-lat/0311027 [hep-lat].
- [26] M. Luscher and P. Weisz, *Commun.Math.Phys.*, **97**, 59 (1985).
- [27] K. Orginos, D. Toussaint, and R. Sugar (MILC Collaboration), *Phys.Rev.*, **D60**, 054503 (1999), arXiv:hep-lat/9903032 [hep-lat].
- [28] J. E. Mandula and M. Ogilvie, *Phys.Lett.*, **B248**, 156 (1990).
- [29] I. Bogolubsky, G. Burgio, M. Muller-Preussker, and V. Mitrjushkin, *Phys.Rev.*, **D74**, 034503 (2006), arXiv:hep-lat/0511056 [hep-lat].
- [30] I. Bogolubsky, V. Bornyakov, G. Burgio, E. Ilgenfritz, M. Muller-Preussker, *et al.*, *Phys.Rev.*, **D77**, 014504 (2008), arXiv:0707.3611 [hep-lat].
- [31] L. Giusti, M. Paciello, C. Parrinello, S. Petrarca, and B. Taglienti, *Int.J.Mod.Phys.*, **A16**, 3487 (2001), arXiv:hep-lat/0104012 [hep-lat].
- [32] M. B. Parappilly, P. O. Bowman, U. M. Heller, D. B. Leinweber, A. G. Williams, *et al.*, *Phys.Rev.*, **D73**, 054504 (2006), arXiv:hep-lat/0511007 [hep-lat].
- [33] J. B. Kogut and L. Susskind, *Phys.Rev.*, **D11**, 395 (1975).
- [34] P. O. Bowman, U. M. Heller, and A. G. Williams, *Phys.Rev.*, **D66**, 014505 (2002), arXiv:hep-lat/0203001 [hep-lat].
- [35] P. O. Bowman, U. M. Heller, and A. G. Williams, *Nucl.Phys.Proc.Suppl.*, **106**, 820 (2002), arXiv:hep-lat/0110081 [hep-lat].
- [36] P. O. Bowman, U. M. Heller, D. B. Leinweber, and A. G. Williams, *Nucl.Phys.Proc.Suppl.*, **119**, 323 (2003), arXiv:hep-lat/0209129 [hep-lat].
- [37] P. O. Bowman, U. M. Heller, D. B. Leinweber, M. B. Parappilly, A. G. Williams, *et al.*, *Phys.Rev.*, **D71**, 054507 (2005), arXiv:hep-lat/0501019 [hep-lat].
- [38] S. Furuï and H. Nakajima, (2005), arXiv:hep-lat/0511045 [hep-lat].
- [39] F. D. Bonnet, P. O. Bowman, D. B. Leinweber, A. G. Williams, and J.-b. Zhang (CSSM Lattice collaboration), *Phys.Rev.*, **D65**, 114503 (2002), arXiv:hep-lat/0202003 [hep-lat].
- [40] J. Zhang, P. O. Bowman, D. B. Leinweber, A. G. Williams, and F. D. Bonnet (CSSM Lattice collaboration), *Phys.Rev.*, **D70**, 034505 (2004), arXiv:hep-lat/0301018 [hep-lat].
- [41] J. Zhang, P. O. Bowman, R. J. Coad, U. M. Heller, D. B. Leinweber, *et al.*, *Phys.Rev.*, **D71**, 014501 (2005), arXiv:hep-lat/0410045 [hep-lat].
- [42] W. Kamleh, P. O. Bowman, D. B. Leinweber, A. G. Williams, and J. Zhang, *Phys.Rev.*, **D71**, 094507 (2005), arXiv:hep-lat/0412022 [hep-lat].
- [43] W. Kamleh, P. O. Bowman, D. B. Leinweber, A. G. Williams, and J. Zhang, *Phys.Rev.*, **D76**, 094501 (2007), arXiv:0705.4129 [hep-lat].
- [44] P. O. Bowman, U. M. Heller, D. B. Leinweber, A. G. Williams, and J. B. Zhang, *Lect. Notes Phys.*, **663**, 17 (2005).
- [45] P. O. Bowman, U. M. Heller, D. B. Leinweber, A. G. Williams, and J.-b. Zhang, *Nucl. Phys. Proc. Suppl.*, **128**, 23 (2004), arXiv:hep-lat/0403002.
- [46] J. I. Skullerud and A. G. Williams, *Phys.Rev.*, **D63**, 054508 (2001), arXiv:hep-lat/0007028 [hep-lat].
- [47] J. Skullerud, D. B. Leinweber, and A. G. Williams, *Phys.Rev.*, **D64**, 074508 (2001), arXiv:hep-lat/0102013 [hep-lat].
- [48] M. Schrock, *Phys.Lett.*, **B711**, 217 (2012), arXiv:1112.5107 [hep-lat].
- [49] C. Itzykson and J. Zuber, *Quantum Field Theory*, International Series In Pure and Applied Physics (Mcgraw-hill, New York, 1980).
- [50] D. B. Leinweber *et al.* (UKQCD), *Phys. Rev.*, **D60**, 094507 (1999), arXiv:hep-lat/9811027.
- [51] A. Voigt, E.-M. Ilgenfritz, M. Muller-Preussker, and A. Sternbeck, *PoS, LAT2007*, 338 (2007), arXiv:0709.4585 [hep-lat].
- [52] C. Popovici, P. Watson, and H. Reinhardt, *Phys.Rev.*, **D79**, 045006 (2009), arXiv:0810.4887 [hep-th].
- [53] N. Cabibbo and E. Marinari, *Phys.Lett.*, **B119**, 387 (1982).
- [54] P. O. Bowman, U. M. Heller, and A. G. Williams, *Nucl.Phys.Proc.Suppl.*, **109A**, 163 (2002), arXiv:hep-lat/0112027 [hep-lat].